Available online at www.sciencedirect.com
SCIENCE DIRECT®
Acta Materialia 52 (2004) 5829–5843
Acta MATERIALIA
www.actamat-journals.com

Two- and three-dimensional equilibrium morphology of a misfitting particle and the Gibbs–Thomson effect

X. Li [a,*], K. Thornton [b], Q. Nie [c], P.W. Voorhees [b], J.S. Lowengrub [c]

[a] Department of Applied Mathematics, Illinois Institute of Technology, 10 West 32nd Street, Chicago, IL 60616, USA
[b] Department of Materials Science and Engineering, Northwestern University, Evanston, IL 60208, USA
[c] Department of Mathematics, University of California, Irvine, CA 92697-3875, USA

Received 13 July 2004; received in revised form 26 August 2004; accepted 30 August 2004
Available online 27 September 2004

Abstract

The equilibrium shapes of misfitting precipitates in elastically anisotropic systems are obtained in both two and three dimensions, and the corresponding Gibbs–Thomson equation is derived as a function of the characteristic ratio between elastic and interfacial energies, L'. The effect of elastic inhomogeneity is investigated systematically. For soft or moderately hard particles, the stable equilibrium shape bifurcates from a fourfold symmetric shape to a twofold symmetric one in 2D and from a cubic symmetric shape to a plate-like one in 3D. For a very hard particle, the shape bifurcation is not observed in 2D for the range of L' investigated, but both plate-like and rod-like shapes are found in 3D. The computed Gibbs–Thomson equation is well approximated by a piecewise linear function of L'. Predictions are made for coarsening of many-particle systems based on an established mean-field theory. The results predict that the elastic stress has no effect on coarsening kinetics where most particles are highly symmetric (fourfold in 2D and cubic in 3D), and the exponent remains 1/3 but the rate constant increases if stress is sufficient to induce symmetry-breaking bifurcation on most particles.
© 2004 Acta Materialia Inc. Published by Elsevier Ltd. All rights reserved.

PACS: 64.70Kb; 81.30Mh
Keywords: Equilibrium shapes; Coarsening; Phase transformations; Alloys

1. Introduction

Microstructural evolution during processing and operation plays a critical role in the macroscopic properties of many technologically important materials. In many multiphase materials, the microstructure consists of second-phase particles embedded in a matrix. The equilibrium morphology of a particle in an infinite matrix helps us understand the factors controlling the morphologies observed in microstructures where many particles are present.

Equilibrium shapes of stress-free particles embedded in another homogeneous phase is well understood. Here, the particle shapes are determined solely by the interfacial energy and have been examined in various literatures including [1–5]. A particle assumes the Wulff shape, which may be obtained through a simple geometric construction that minimizes the total surface energy of a particle with fixed volume. On the other hand, when elastic stress is present, the construction of an equilibrium shape is a complex task, involving the minimization of the *sum* of the interfacial and elastic energies. The resulting equilibrium shapes are often not simple geometric shapes (like a sphere or spheroid), and thus obtaining such shapes relies on numerical approaches. In addition, while the equilibrium shape of a stress-free

* Corresponding author. Tel.: +1 312 567 5340; fax: +1 312 567 3135.
E-mail address: lix@iit.edu (X. Li).

1359-6454/$30.00 © 2004 Acta Materialia Inc. Published by Elsevier Ltd. All rights reserved.
doi:10.1016/j.actamat.2004.08.041

particle is independent of the particle size, this is not the case when misfit stress is present (as in solid two-phase coherent alloys). Since the relative importance of elastic energy to interfacial energy increases with particle size, the equilibrium shape must be determined as a function of the particle size, or alternatively, of the relative importance of these two energies.

We here consider elastically anisotropic systems similar to those used in high temperature alloys since many materials possess anisotropic elastic properties reflecting their crystallographic structure. In two dimensions, Thompson et al. [6] studied the equilibrium shapes of misfitting second-phase particles for elastically homogeneous, cubic systems. To characterize the relative importance of elastic energy compared to interfacial energy, they used the parameter $L \equiv \varepsilon^2 C_{44} l/\sigma$ introduced in [7], where ε is the magnitude of the misfit strain, which is assumed to be dilatational and independent of composition, C_{44} is an elastic constant for the solid (assumed equal in the matrix and the precipitate phases), in which there are three independent components for a cubic system, and σ is the constant surface energy per unit length. The characteristic length l is determined by the equivalent radius of the precipitate, $r = (A/\pi)^{1/2}$, where A is the area of the particle. Note that the parameter L does not reflect the elastic inhomogeneity, thus, in Section 2, we introduce a new parameter L' for inhomogeneous systems. Thompson et al. [6] found that the equilibrium shape changes from a circle (of stress-free particle) to a fourfold symmetric shape, approximately square with rounded corners, as L increases, and at a critical value of L, L_c, the particle shape bifurcates to a twofold symmetric shape elongated along the elastically soft directions.

Inhomogeneity in elastic properties (i.e., the elastic constants are different in the matrix and the particles) introduces further complications. Both the equilibrium shapes and the critical value of L at which the bifurcation occurs depend on elastic inhomogeneity [8–11]. When elastic homogeneity is assumed in 2D, there exists a Green's function which allows the displacement field to be calculated via integration along the interface [6]. When the elastic constants are different, two coupled integral equations corresponding to the elastic equations must be solved for the displacement and traction fields even though there exist explicit expressions for Green's functions. Jou et al. [8], Schmidt et al. [9,10], and Leo et al. [11] have examined elastically inhomogeneous systems using the boundary integral method in 2D.

In three dimensions, there have been analytical studies examining energy-minimizing shapes restricting the shapes to a certain type [12–14]. These results will not give true equilibrium shapes for which the chemical potential on the surface is constant. Nevertheless, Johnson and Cahn [15] were able to show that particle shape bifurcations are possible and determined analytically the structure of the bifurcation within the class of spheroidal shapes.

Recently, numerical studies have been conducted imposing no restrictions on the shape of the particles. Application of boundary integral method becomes even more challenging for three-dimensional anisotropic elasticity. The Green's function must be evaluated numerically since explicit expressions of the Green's function are not available. Thompson and Voorhees [16] have studied the equilibrium shapes in 3D with homogeneous, cubic elasticity by energy minimization. Using a configurational force, Mueller and Gross [17–19] have calculated 3D equilibrium shapes for inhomogeneous systems. The equilibrium shapes of periodically arranged particles have been computed using a boundary integral method by Mueller and coworkers [20] and Eckert et al. [21] and using a phase-field method by Zhu et al. as well [22]. Li et al. [23] examined both the equilibrium shape and the dynamics of the morphological evolution of a precipitate in an elastically anisotropic, inhomogeneous medium. Using a boundary element method, along with the adaptive surface mesh algorithm developed by Cristini et al. [24], they found an equilibrium shape of tetragonal symmetry for a Ni_3Al precipitate in a nickel matrix in the absence of external loading.

In all of these studies, the focus was on the equilibrium shapes or the dynamics, and not on the interfacial concentration when a equilibrium shape is attained. The interfacial concentration of an equilibrium shape is constant along the interface, and thus it is a single value for the equilibrium. For a stress-free system with isotropic interfacial energy, a sphere is the equilibrium shape, and the interfacial concentration is a sole function of the radius of the sphere for a given interfacial energy. The equation that provides the interfacial concentration (for example, as a function of the interfacial curvature or the radius of the particle) is called the Gibbs–Thomson equation. The significance of the Gibbs–Thomson equation lies in that it provides the boundary condition at the interface for a solution to the diffusion equation in the sharp interface description of both single and multiple particle systems [25]. Thus, it is often used to understand growth and coarsening in multiphase systems. In particular, in stress-free systems the Gibbs–Thomson equation takes a very simple form, $C(R) \propto 1/R$, where C and R are the dimensional concentration and the dimensional particle radius, respectively. Such an equation is used to study coarsening kinetics of second-phase particles, and, when combined with the steady state diffusion equation and mass conservation, yields the well-known $t^{1/3}$ power-law for the average particle size.

In a system where stress is important, the Gibbs–Thomson equation becomes very complex since the equilibrium particle shape is not given by a simple geometric shape; the interfacial concentration is therefore

obtained numerically. In addition, a priori, we do not know if elastic interactions may have a significant effect on the coarsening since it depends not only on the volume fraction but also on the elastic constants of the two phases and the microstructure. Thus, for a two-dimensional, elastically homogeneous system, Thornton et al. [26–28] performed a large-scale simulation of the coarsening process using boundary integral methods. They examined the temporal evolution of the average circularly equivalent radius $\langle R\rangle$ and found that, $\langle R\rangle^3 = Kt$, where K is the rate constant, just as in the absence of stress. Moreover, when the particles are small enough such that the particles are fourfold symmetric, the rate constant K is equal to that in the absence of stress. Thus, when the particle is fourfold symmetric, elastic stress has no effect on the rate of coarsening when $\langle R\rangle$ is used to characterize the length scale in the coarsening process. Furthermore, when the majority of the particles become large enough such that most particles have undergone a shape bifurcation to twofold symmetric shapes, the temporal exponent remains 1/3, but the rate constant K increases. The two regimes are bridged by a smooth crossover where fourfold and twofold symmetric particles both have significant presence. They identified the source of the increase in K as a change in the equilibrium interface concentrations accompanying the change in morphology from fourfold to twofold shapes [26,28]. In particular, they found that the equilibrium concentration of an isolated particle can be described as

$$C = C_\infty^\alpha\left(1 + a\frac{l_c}{R} + b\frac{l_c\varepsilon^2 C_{44}}{\sigma}\right), \tag{1}$$

where C_∞^α is the equilibrium concentration at a planar interface in the matrix phase in a stress-free system, l_c is the capillary length in the absence of stress, and a and b are constants that depend on the elastic constants ($a = 1$ and $\varepsilon = 0$ recovers the Gibbs–Thomson equation for a stress-free circular particle). Thus, the elastic stress changes the driving force for coarsening by the factor, a. The Gibbs–Thomson equation is a function only of the symmetry of the equilibrium particle shape, not the actual shape of the particle at a given L. Using this insight, the analytical theory of Marqusee [29] on the coarsening process for stress-free systems was extended to include elastic effects. The theory, which is consistent with the numerical simulations, predicts that

$$\langle R\rangle^3 = aDA_m f(\phi) l_c C_\infty^\alpha t, \tag{2}$$

where D is the diffusion coefficient, A_m is the molar area (in 2D) or volume (in 3D), and $f(\phi)$ gives the dependence of the coarsening rate on volume fraction in the absence of stress. The effects of elastic stress are contained in the coefficient a appearing in the stress-modified Gibbs–Thomson equation, Eq. (1). For a fourfold symmetric particle of equilibrium shape, $a = 1$, whereas for a twofold symmetric particle $a > 1$, with the exact value depending on the elastic properties of the system [28]. Thus, if most of the particles are fourfold symmetric, the coarsening rate will be exactly the same as that in the absence of stress, and when most of the particles are twofold symmetric the coarsening rate will be higher, assuming that elastic interactions do not bias coarsening. A similar theory can be developed for a three-dimensional system based on the mean-field theory of Marqusee and Ross [30], resulting in the same conclusion.

In this work, we will obtain the concentration on an isolated precipitate interface at equilibrium state for a wide range of materials, both elastically homogeneous and inhomogeneous, in two and three dimensions, and discuss its implications on the prediction of the coarsening kinetics without performing large scale simulations.

The paper is organized as follows. In Section 2, we state the problem, the governing equations, and the solution procedure. In Section 3, we present the numerical results, including the equilibrium shapes for two- and three-dimensional isolated precipitate in an infinite matrix and the Gibbs–Thomson relation as a function of L', and we examine the effect of elastic inhomogeneity. In Section 4, we compare the results from two-dimensional and three-dimensional systems, discuss the significance of the elastic interactions among particles and summarize our findings.

2. Governing equations

We investigate the equilibrium states of an isolated precipitate in an infinite matrix. The two phases are separated by a closed sharp interface (the Gibbs dividing surface) S. Equilibrium is reached through the diffusional flow of mass in the bulk, governed by Laplace's equation, $\nabla^2 c = 0$, and the boundary condition is given by the generalized Gibbs–Thomson relation

$$c = \kappa + L' g^{el} \quad \text{on} \quad S, \tag{3}$$

where c is the dimensionless concentration, κ is the curvature (in 2D) or the sum of the principle curvatures (in 3D) of the interface, and g^{el} is the dimensionless elastic energy density. To characterize the ratio of elastic energy and surface energy of an elastically inhomogeneous system, we introduce a new dimensionless parameter L' defined by

$$L' \equiv \frac{\overline{g^{el}}\, l}{\sigma}, \tag{4}$$

where $\overline{g^{el}}$ is a characteristic dimensional strain energy density. For a homogeneous system, $\overline{g^{el}}$ is chosen to be $C_{44}^M\varepsilon^2$ as in [7], making L' identical to L defined earlier, where C_{44}^M denotes the elastic constant C_{44} in the matrix. In an inhomogeneous system, however, the original

nondimensional parameter L from [7] does not take into account changes in the elastic energy due to inhomogeneity. Thus, inhomogeneous systems that have the same value of L may in fact have different ratios of elastic to surface energies which can lead to significantly different microstructure morphologies. Here, L' is introduced to scale out this effect of inhomogeneity. In particular, $\overline{g^{\mathrm{el}}}$ is taken to depend on the elastic constants of both phases such that L' reflects more accurately ratio of elastic to surface energies in an inhomogeneous system. This is accomplished as follows. Since elastic energy depends on size and particle morphology, $\overline{g^{\mathrm{el}}}$ is defined as $C_{44}^{\mathrm{M}}\varepsilon^2$ multiplied by the ratio of the elastic energies of the inhomogeneous system and the corresponding homogeneous system for a circular (in 2D) or spherical (in 3D) precipitate of unit radius embedded in an infinite matrix. Thus, the ratios of the elastic and the surface energies $W_{\mathrm{e}}/W_{\mathrm{s}}$ are identical for the same value of the new parameter, L', regardless of the inhomogeneity of systems containing a circular or spherical particle of unit radius. Although the particles we consider in this work are generally not circular or spherical, we find that this scaling nevertheless enables us to examine the effect of inhomogeneity for nearly fixed elastic to surface energy ratios. Finally, as will be discussed later in Section 3, for a special class of inhomogeneous systems, an explicit expression of $\overline{g^{\mathrm{el}}}$ can be obtained.

The non-dimensionalization of the variables follows [31,32] except that the stress is scaled by $\overline{g^{\mathrm{el}}}/\varepsilon$ instead of $C_{44}^{\mathrm{M}}\varepsilon$. Note, in three dimensions, the characteristic length l is determined by the spherically equivalent radius $R = (V/(4\pi/3))^{1/3}$, where V is the volume of the precipitate. The energy density g^{el} is expressed in terms of the scaled strain and dimensionless stress tensors, $\boldsymbol{\varepsilon}$ and $\boldsymbol{\sigma}$, respectively, on both sides of the coherent interface

$$g^{\mathrm{el}} = \tfrac{1}{2}\left(\boldsymbol{\sigma}^{\mathrm{P}}\cdot\left(\boldsymbol{\varepsilon}^{\mathrm{P}}-\boldsymbol{\varepsilon}^{\mathrm{T}}\right)-\boldsymbol{\sigma}^{\mathrm{M}}\cdot\boldsymbol{\varepsilon}^{\mathrm{M}}\right)+\boldsymbol{\sigma}^{\mathrm{M}}\cdot\left(\boldsymbol{\varepsilon}^{\mathrm{M}}-\boldsymbol{\varepsilon}^{\mathrm{P}}\right)\ \text{on } S, \tag{5}$$

where we denote the variables defined in the matrix or in the precipitate by the superscript M or P, respectively.

The motion of the interface is governed by the flux balance $v_n = [\![\frac{\partial c}{\partial n}]\!]$ where v_n is the magnitude of the normal velocity of the precipitate–matrix interface, $[\![f]\!] \equiv f|_{S^+} - f|_{S^-}$ denotes the jump of a quantity f from the precipitate side to the matrix side of the interface, n is the coordinate along the normal of the interface pointing into the particle, and we have assumed that the diffusion coefficients in the matrix and particle phases are identical. The far-field condition for the diffusion problem reflects zero mass flux into the system, $\int_S v_n \mathrm{d}A = 0$.

From Eq. (5), one realizes that obtaining g^{el} requires solving the elasticity equation $\nabla\cdot\boldsymbol{\sigma} = 0$ both in Ω^{P}, the domain occupied by the precipitate, and in the matrix, Ω^{M}. The interface between the two phases S is taken to be coherent and the elastic stress exists due to the presence of mismatch in lattice spacing between the two different phases. The misfit strain is assumed purely dilatational, $\boldsymbol{\varepsilon}^{\mathrm{T}} = \mathbf{I}$, where $\mathbf{I}$ is the identity matrix.

The total energy of the system, W_{tot}, is the sum of the surface energy, W_{s}, and the elastic energy, W_{e}, where

$$W_{\mathrm{s}} = \int_S \mathrm{d}A,$$
$$W_{\mathrm{e}} = \frac{L'}{2}\left[\int_{\Omega^{\mathrm{P}}}\boldsymbol{\sigma}^{\mathrm{P}}\cdot\left(\boldsymbol{\varepsilon}^{\mathrm{P}}-\boldsymbol{\varepsilon}^{\mathrm{T}}\right)\mathrm{d}V+\int_{\Omega^{\mathrm{M}}}\boldsymbol{\sigma}^{\mathrm{M}}\cdot\boldsymbol{\varepsilon}^{\mathrm{M}}\,\mathrm{d}V\right]. \tag{6}$$

Here, we briefly describe the solution procedure for evolving the shape of the precipitate. The details are presented in [11] for the two-dimensional simulations and in [23] for the three-dimensional case.

Both the diffusion equation and the elasticity equation can be reformulated in boundary integral equations, which are solved by a boundary integral method in 2D [11] and a boundary element collocation method with adaptive surface mesh in 3D [23,24]. The position of the interface is traced by a set of marker points on the interface $\{\mathbf{x}_i\}$, $i = 1,\ldots,N$, where N is the total number of mesh points. Requiring the integral equations be satisfied at these marker points reduces the integral equations to linear systems. Since the corresponding coefficient matrices are dense and non-symmetric, the GMRES method is applied to solve the discretized linear equations.

At each time-step, the discretized elasticity equations are solved to obtain the boundary condition for the diffusion equation. The normal velocity is acquired by solving the discretized integral equation corresponding to diffusion, and the marker points are evolved by the differential equation, $\mathrm{d}\mathbf{x}/\mathrm{d}t = v_n\mathbf{n}$. The simulation of the evolution is stopped, when the precipitate reaches an equilibrium shape, in particular, as the variation in the concentration c on the surface of the precipitate is less than 0.02% of the average value of c.

3. Results

In this section, we present the numerical results on the equilibrium states of homogeneous and inhomogeneous media in two and three dimensional dimensions. We consider an isolated precipitate in an infinite matrix. Both the matrix and the precipitate phases have cubic elasticity, and the three independent parameters in the dimensionless elastic constant tensor for the matrix are given by those of nickel, C^{M}: $c_{11}^{\mathrm{M}} = 1.98, c_{12}^{\mathrm{M}} = 1.18$, and $c_{44}^{\mathrm{M}} = 1$. The isolated particle evolves according to the diffusional processes described by the quasi-steady diffusion equation and the generalized Gibbs–Thomson boundary condition, Eq. (3). The total energy, W_{tot},

given in Eq. (6), decreases during the evolution. The system reaches an equilibrium state when the total energy reaches an extremum.

3.1. Accuracy of numerical simulations

In most of our two-dimensional calculations, the matrix–precipitate interface is represented by 512 marker points. We find that the equilibrium shapes are indistinguishable if the number of marker points is increased to 1024. The constant concentration values at equilibrium obtained from the two resolutions are identical to the eighth and the third significant figure for fourfold and twofold symmetric shapes, respectively. For a detailed account on the performance of the numerical methods, see the work by Leo et al. [11].

For three-dimensional simulations, Fig. 1 shows the x–y plane cross-sections of the equilibrium shapes of a three-dimensional precipitate in an inhomogeneous system at different resolutions. The mesh size for the dashed-line contour has 204 triangles on the surface, while the dotted and the solid lines correspond to finer mesh sizes of 408 and 816 triangles, respectively. The small difference in the equilibrium shapes of different mesh sizes demonstrates the accuracy of our methods. Furthermore, the dimensionless concentration c of a particle with unit equivalent radius at equilibrium is $c(h) = 2.8094$ for the coarse mesh, $c(h/\sqrt{2}) = 2.8011$ for the median mesh size, and $c(h/2) = 2.7978$ for the fine mesh. The concentration data implies that the order of convergence of the methods is between $O(h^2)$ and $O(h^3)$. The result shown in Fig. 1 is representative of our three-dimensional simulations of inhomogeneous systems. In this work, the three-dimensional results have been obtained with the mesh size similar to the median size displayed in Fig. 1. For further discussion on the performance of the numerical schemes, refer to [23].

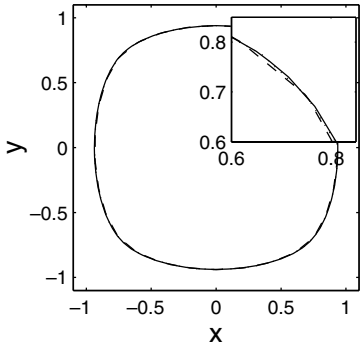

Fig. 1. Convergence test: the cross-sections of the equilibrium shapes of a three-dimensional precipitate in the elastically inhomogeneous system [Ni–Ni0.5] at $L' = 1.44$ ($L = 2$) for different mesh sizes: a coarse mesh with 204 triangles (the dashed line), a median-sized mesh with 408 triangles (the dotted line) and a fine mesh with 816 (the solid line). A selected region of the cross-sections is magnified and also shown in the figure. The dotted line almost overlaps the solid line.

3.2. L': the scaled ratio of elastic to interfacial energies

In order to study the effect of inhomogeneity systematically, the elastic constants of the precipitate are obtained by multiplying those of the matrix phase, nickel, by a constant factor $1/\psi$ where $\psi \equiv C_{44}^{M}/C_{44}^{P}$. For example, [Ni–Ni0.9] refers to the inhomogeneous system where the elastic constants of the precipitate are those of nickel multiplied by the factor $1/\psi = 0.9$, i.e., $C^{P} = 0.9C^{M}$.

The characteristic scale for the elastic energy density $\overline{g^{el}}$ in the definition of L', Eq. (4), depends on the elastic energy W_e for a circular (in 2D) or spherical (in 3D) particle of unit radius. For the special case where $C^{P} = C^{M}/\psi$, we find [1] that the dependence of the elastic energy on inhomogeneity is given by $W_e(\psi) = \frac{1+B}{1+\psi B} W_e(\psi = 1)$, where the parameter B is a homogeneous function of the elastic constants C^{P}. We find that the parameter B is independent of ψ: $B \approx 0.628$ in 3D and $B \approx 0.389$ in 2D for the nickel constants chosen in this work. Thus, in this special class of elastic inhomogeneities, the characteristic strain energy density $\overline{g^{el}}$ and the nondimensional parameter L', characterizing the relative effects of elastic and surface energies, introduced in Section 2 can be explicitly expressed as

$$\overline{g^{el}} = \frac{1+B}{1+\psi B}\varepsilon^2 C_{44}^{M} \quad \text{and} \quad L' = \frac{1+B}{1+\psi B}\frac{\varepsilon^2 C_{44}^{M} l}{\sigma} = \frac{1+B}{1+\psi B} L. \tag{7}$$

3.3. The equilibrium shapes of a misfitting particle

3.3.1. Two-dimensional simulations

In this work, the equilibrium states are obtained through dynamic simulations. For each value of L', two simulations are performed, one starting from a precipitate having the shape of the unit circle, the other from the shape of an ellipse with area π given by the equations $x = (3/2)\cos\theta$ and $y = (2/3)\sin\theta$.

The equilibrium shapes of a two-dimensional misfitting particle as a function of L', their stability and the effect of inhomogeneity on the shapes have been discussed in [6,8,9,11]. In two dimensions, we will focus our discussion on the Gibbs–Thomson relation later in this section, and here we summarize the related results on equilibrium shapes for completeness and better

[1] For the system of a precipitate with the shape of the unit sphere and isotropic elastic constants μ^{P} and K^{P} in an infinite matrix with μ^{M} and K^{M}, Leo [33] gives the expression for the elastic energy $W_e = 8\pi L \varepsilon_{ii}^{T} \mu^{M}/(1 + \frac{4}{3}\frac{\mu^{P}}{K^{P}}\psi)$. Our expression of W_e is derived from that of the isotropic elasticities and has been verified numerically.

understanding of the corresponding three-dimensional results followed.

For an elastically cubic system with dilatational misfit, the equilibrium shape of a precipitate depends on the value of L': for small values of L', it is fourfold symmetric and circular or squarish; when the value of L' is larger than a critical value, denoted by L'_c, there exist at least two types of equilibrium shapes, one remains fourfold symmetric and the other is twofold symmetric and rectangular. Examples of these two kinds of shape are shown in Fig. 6(b). For each value of L' less than L'_c, the fourfold symmetric equilibrium is unique and minimizes the total energy; for $L' > L'_c$, the twofold symmetric equilibrium is stable and possesses the minimum total energy, but the fourfold symmetric one is unstable and is a saddle point in total energy. Thompson et al. [6] constructed the bifurcation diagram for the parameter L' and showed the symmetry-breaking bifurcation is supercritical for the homogeneous systems. To date, the corresponding bifurcation diagram for the inhomogeneous systems is not complete.

Inhomogeneity has significant effect on the equilibrium shapes: the fourfold symmetric equilibrium shapes become more rounded as the hardness of the precipitate increases with respect to that of the matrix phase; the aspect ratios of the twofold symmetric equilibrium shapes increases as the precipitate becomes softer. The estimation of the shape bifurcation value L'_c for various systems can be looked up in Fig. 8(d) presented later in Section 3.4. L'_c is an increasing function of the hardness of the precipitate, indicating that a harder precipitate will bifurcate to twofold symmetric shapes at higher ratio of elastic energy to surface energy. Note that in 2D, for [Ni–Ni1.5], where the precipitate is elastically much harder than the matrix, the estimate of L'_c is not given since the equilibrium shape retains fourfold symmetry for the values L' up to 33.1. The more accurate estimation of L'_c is difficult to obtain through dynamic simulations since the evolution toward equilibrium becomes extremely slow near the bifurcation point, and thus they are not investigated. Our results are consistent with those obtained by Schmidt and Gross [9] after converting their results in terms of L' defined by Eq. (7).

3.3.2. Three-dimensional simulations

The initial shapes in three-dimensional simulations are obtained from the equilibrium shapes for smaller values of L'. For each combination of the matrix and the precipitate phases, we compute the equilibrium shape for the smallest value L' starting with the initial shape of a unit sphere; incrementing L', we calculate the series of equilibrium shapes using the equilibrium shape calculated for the previous step in L' as the initial shape; we continue to increment L' and obtain the steady states until the computation becomes too costly to perform due to the large number of meshes required.

Fig. 2 shows equilibrium shapes of a three-dimensional precipitate with unit equivalent radius for different values of L' in the homogeneous system [Ni–Ni], where the elastic constants of the two phases are equal $C^P = C^M$. Again, in a homogeneous system, the scaled parameter L' is identical to L. When $L' = 1$, Fig. 2(a) shows that the equilibrium shape is similar to a sphere which is the shape that minimizes the surface energy, but with somewhat flatter faces and rounded edges and corners. Figs. 2(b) and (c) show steady states just before and after the shape bifurcation for $L' = 3$ and 4 respectively. At $L' = 3$, the shape clearly forms a flat face perpendicular to each of the three mutually perpendicular elastically soft directions of the cubic anisotropy, $\langle 1\,0\,0\rangle$, and retains cubic symmetry. When $L' = 4$, our calculations show that the equilibrium shape with cubic symmetry is unstable, and the stable equilibrium shape attains a plate-like shape, as shown in Fig. 2(c). Here, a *plate* refers to a shape with tetragonal symmetry in which the side along the fourfold-symmetry axis is shorter than the other sides. In contrast, a *rod* has the side along the fourfold-symmetry axis that is longer than the other sides. As L' increases further to 8, the equilibrium shape becomes a flatter plate as shown in Fig. 2(d). This is consistent with the analytic result [34,35] that predicts the equilibrium shape becomes an infinitely thin plate for an elastically homogeneous system as L' goes to infinity. Note that the maximum curvature of the equilibrium shapes increases as the value of L' is raised. Correspondingly, the size of surface mesh increases adaptively to resolve the high curvature area [24]. For example, to achieve the same accuracy, 362 and 3834 mesh points are needed for $L' = 1$ and $L' = 8$, respectively. The computational cost increases dramatically when L' is large because the cost for each time-step increases as $O(N^2)$ where N is the number of the surface mesh points, and, furthermore, numerical stability requires a smaller time step.

Next, we examine the effect of inhomogeneity on the equilibrium shapes in 3D, using L' instead of L to characterize the ratio of elastic energy and surface energy for an elastically inhomogeneous system. For $L' = 2$, Fig. 3 shows the equilibrium shapes of a soft precipitate in [Ni–Ni0.5] (Fig. 3(a)), a precipitate in an elastically homogeneous system [Ni–Ni] (Fig. 3(b)) and a hard precipitate in [Ni–Ni1.5] (Fig. 3(c)). The cross-sections of the three shapes in the x–y coordinate plane are plotted together in Fig. 3(d). Since the same value of L' represents the same ratio of elastic energy and the surface energy for a unit sphere regardless the inhomogeneity, the equilibrium shapes of these precipitates in systems with drastically different elastic inhomogeneities are all cubic symmetric and have similar dimensions for this relatively small value of L'. However, as shown in the cross-sections, the differences are visible, showing the softer precipitate has sharper

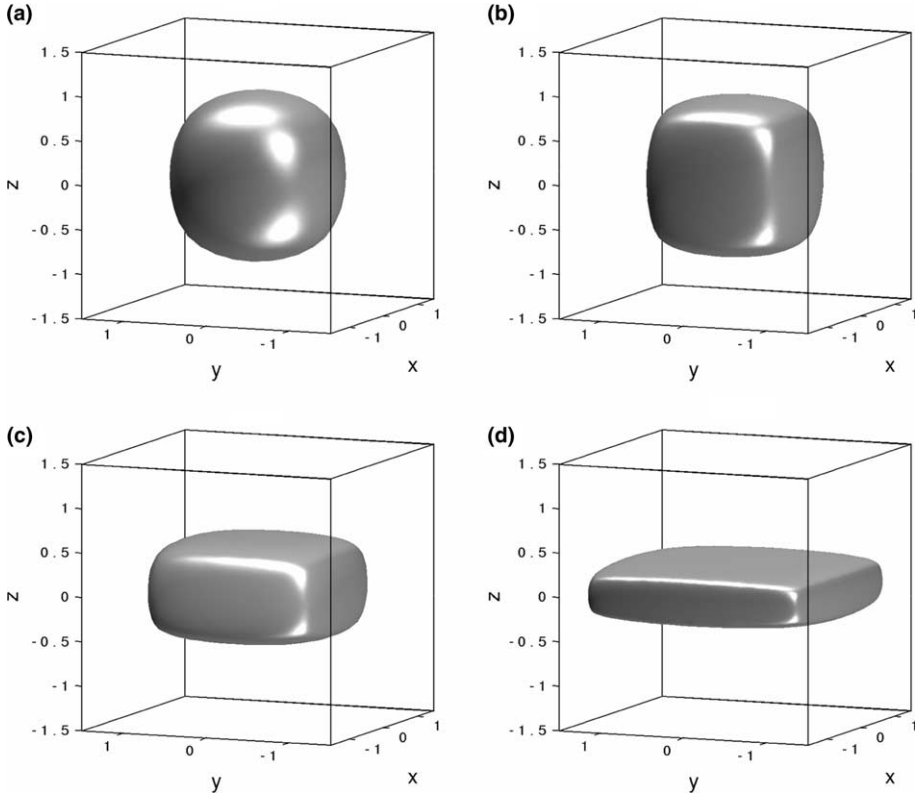

Fig. 2. Equilibrium shapes of a precipitate in the homogeneous [Ni–Ni] system for (a) $L' = 1$, (b) $L' = 3$, (c) $L' = 4$ and (d) $L' = 8$.

edges and flatter faces. This is different from our 2D result at the same L' (not shown here) where the differences in the equilibrium shapes are undetectable. The disagreement may be due to the fact that, at the same value of L', the ratio of elastic energy to surface energy in 3D is greater than that in 2D. In fact, as shown later in Section 4, $L' = 2$ in 3D corresponds to $L' \approx 3.7851$ in 2D. At a larger value of $L' = 5$, the equilibrium shapes in the different systems ([Ni–Ni0.5], [Ni–Ni], [Ni–Ni1.1] and [Ni–Ni1.5]) are distinct from each other, as shown in Fig. 4. For soft precipitate and moderately hard precipitate, the equilibrium shapes in Fig. 4(a)–(c) are the bifurcated plate-like shape with tetragonal symmetry, and the aspect ratio of the particle dimensions (the longer dimension over the shorter one) increases as the precipitate becomes softer. For the hardest particle in [Ni–Ni1.5] and $L' = 5$, the equilibrium shape has not bifurcated and remains cubic symmetric as shown in Fig. 4(d).

For the homogeneous and inhomogeneous systems where the precipitate is softer to moderately harder than the matrix, the equilibrium shape is cubic symmetric for small L', and is plate-like after the bifurcation. However, for the case of very hard precipitate [Ni–Ni1.5], the stable equilibrium shape is a cubic symmetric shape (Fig. 4(d)) for $0 < L' < 6.8$ ($0 < L < 6$), becomes a plate-like shape with small aspect ratio of 1.104 (Fig. 5(a)) at an L' between 6.8 and 8.0 (L between 6 and 7), and then changes to a rod-like shape (Fig. 5(b)) at an L' between 8.0 and 9.2 (L between 7 and 8).

Using configurational forces for microstructural evolution, Mueller and Gross [17–19] studied the effects of L and the inhomogeneity on equilibrium shapes of three-dimensional precipitates *with cubic symmetry*. Our results, obtained by a diffusional process, are consistent with their findings prior to the shape bifurcation point. Since the bifurcated shapes in absence of external loading were not discussed in their work, a more detailed comparison cannot be made.

3.4. The Gibbs–Thomson equation as a function of L'

As described in Section 1, based on Marqusee's mean-field theory for stress-free systems [29], Thornton et al. [26] developed an analytical theory for the coarsening process where the effects of elastic stress on the coarsening rate can be accounted for by the Gibbs–Thomson equation with elastic effects, which can be approximated by the constant concentration c along the interface of an isolated precipitate at equilibrium. The theory motivates us to study the dependence of c on the dimensionless parameter L'.

In this paper, we compute the concentration c when the precipitate evolves to an equilibrium state for different values of L'. The misfit strain is purely dilatational and elastic inhomogeneity is confined to have the

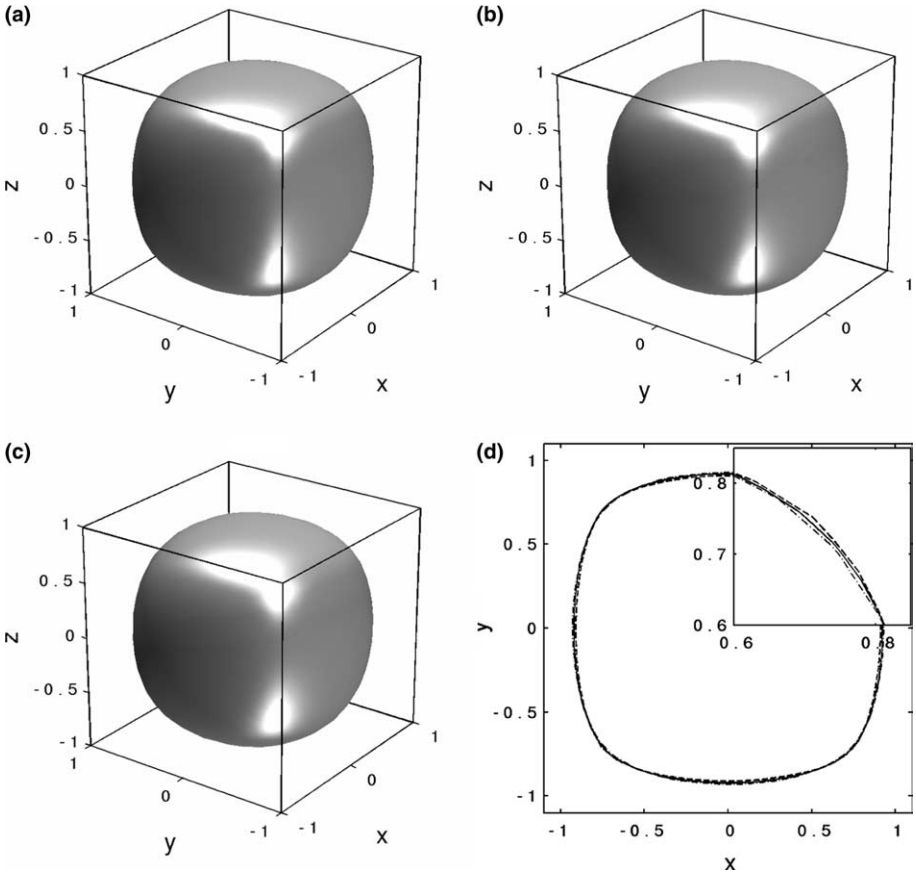

Fig. 3. Equilibrium shapes of a precipitate at $L' = 2$ in (a) the elastically inhomogeneous system with a soft particle [Ni–Ni0.5], (b) the homogeneous system [Ni–Ni], and (c) the inhomogeneous system with a hard particle [Ni–Ni1.5]. (d) The cross-section in x–y plane of the three precipitates at equilibrium in [Ni–Ni] (shown with the solid line), [Ni–Ni0.5] (the dashed line) and [Ni–Ni1.5] (the dash-dotted line) systems. A magnified region is also plotted.

property $C^P = C^M/\psi$ where $1/\psi = 0.5$, 0.9, 1, 1.1, and 1.5. The dependence of c as a function of L' is plotted in Figs. 6 and 7 for the two- and three-dimensional systems, respectively.

Independent of the dimensionality (2D or 3D) and elastic inhomogeneity, our results show that the Gibbs–Thomson equation for a particle with unit equivalent radius at equilibrium is *always* well approximated by a piecewise linear function of L' for the range of L' studied

$$c' \equiv c/\kappa_0 = \begin{cases} 1 + b_1 L' & \text{if} \quad L' < L'_c, \\ a_2 + b_2 L' & \text{if} \quad L' > L'_c, \end{cases} \tag{8}$$

where the constant κ_0 is defined such that $c' = 1$ when $L' = 0$, i.e., $\kappa_0 = 1$ in 2D and $\kappa_0 = 2$ in 3D. Thus, $c' = c$ for 2D. Note that, since the scaling parameter in Eq. (7) is a constant for a fixed system, the relation between c and L in their original definitions remains approximately piecewise linear. This piecewise linear relation between c' and L' was first discovered in a two-dimensional, elastically homogeneous system by Thornton et al. [26]. In addition, from the generalized Gibbs–Thomson relation (3), the value of c' at equilibrium increases from one to infinity as L' is raised from zero to infinity.

Because of the piecewise linear relation, we can calculate the value of L' where the two linear functions intersect

$$L'_i \equiv \frac{1 - a_2}{b_2 - b_1}, \tag{9}$$

and L'_c is the bifurcation point beyond which the equilibrium shape bifurcates to a shape with less symmetry. Although, in principle, the values of L'_c and L'_i could be different, there is evidence that the two values are close. For two-dimensional elastically homogeneous systems, we find that L'_i provides a upper bound for L'_c and the difference between the two values indeed is small when the anisotropic ratio $A_r \equiv 2c_{44}/(c_{11} - c_{12})$ is not large ($A_r < 4.5$). Since the value of A_r for Ni constants in our simulations is 2.5, the bifurcation point L'_c can be approximated by the value of L'_i. The value of the intersection point L'_i can be extracted from a few values of the constant concentration c' away from the bifurca-

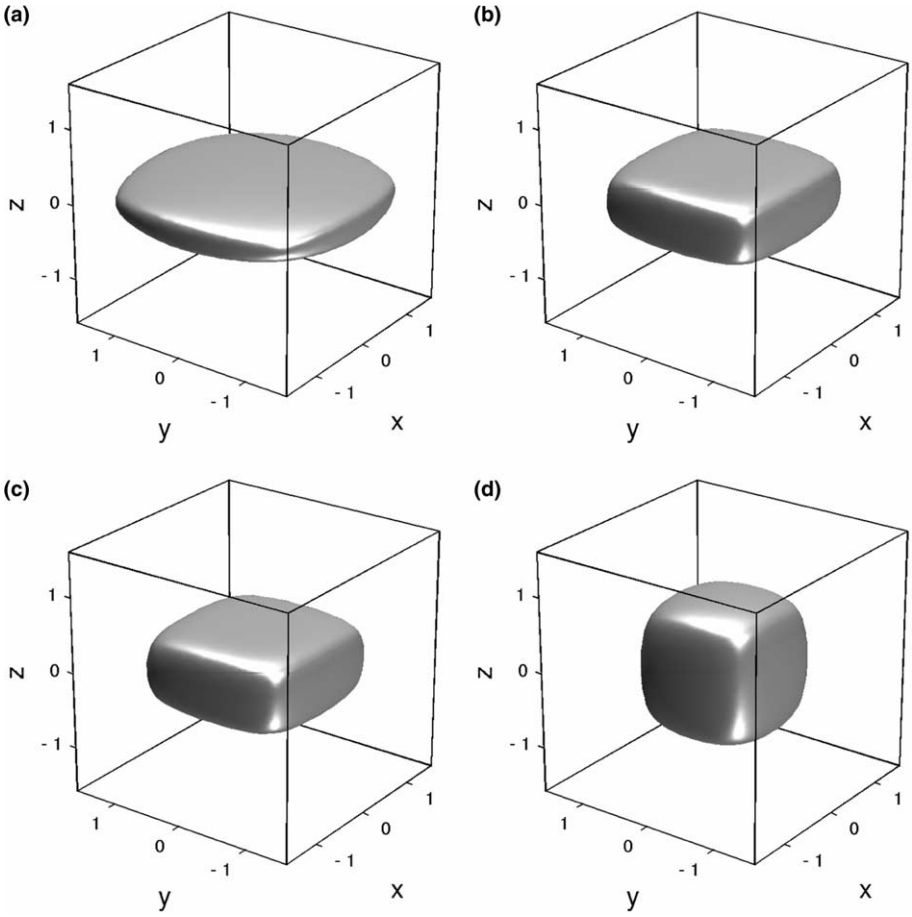

Fig. 4. Equilibrium shapes of a precipitate at $L' = 5$ in (a) the elastically inhomogeneous system with a soft particle [Ni–Ni0.5], (b) the homogeneous system [Ni–Ni], (c) the inhomogeneous system with a hard particle [Ni–Ni1.1], and (d) the inhomogeneous system with a hard particle [Ni–Ni1.5].

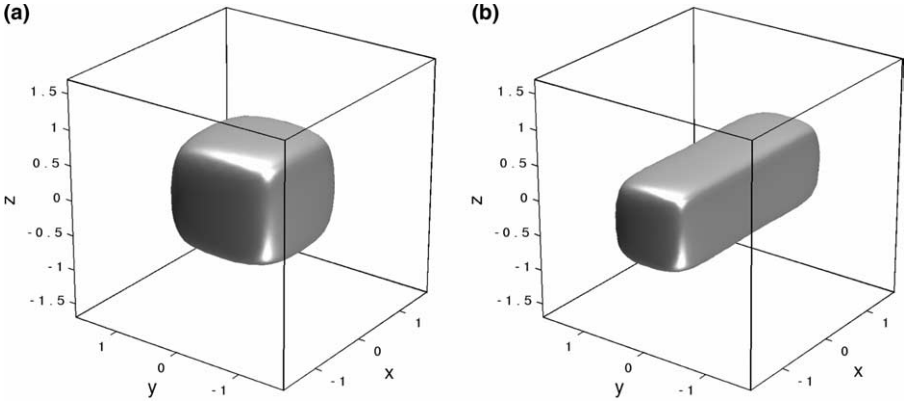

Fig. 5. Equilibrium shapes of a hard precipitate in the inhomogeneous system [Ni–Ni1.5] at (a) $L' = 8.03$ ($L = 7$) and (b) $L' = 12.6$ ($L = 11$).

tion. Consequently, the bifurcation point L'_c can be estimated without a full scale computation of the equilibrium states for values of L' near the bifurcation.

The bifurcation point L'_c, the intersection value L'_i and the constants b_1, a_2 and b_2 depend on the elastic constants. In this work, we will investigate the dependence of these constants on the dimensionality and the elastic inhomogeneity. The summary of the results is given in Fig. 8.

3.4.1. Two-dimensional systems

The dimensionless concentration c' as a function of L' is graphed in Fig. 6, where the computed data are indicated by the circles and the crosses. The least-square

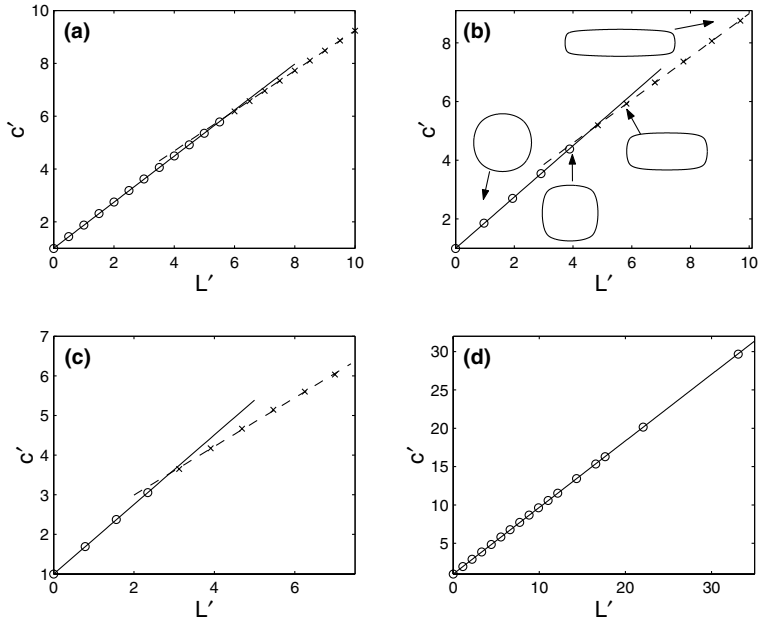

Fig. 6. Dimensionless concentration c' as a function of L' for two-dimensional systems. (a) [Ni–Ni]; (b) [Ni–Ni0.9] (the equilibrium shapes for various values of L' are also shown); (c) [Ni–Ni0.5]; (d) [Ni–Ni1.5]. The circles and the crosses represent the data points before and after the shape bifurcation, respectively. The solid and dashed lines give the least-square fit of the data points.

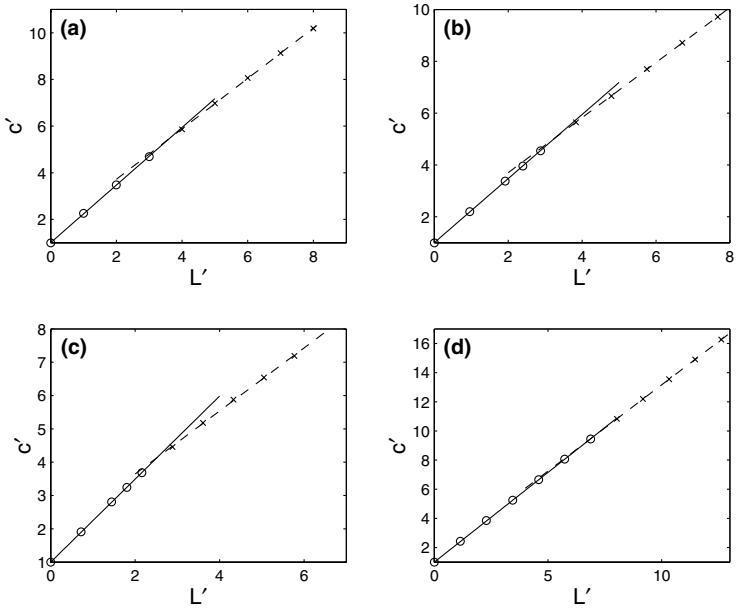

Fig. 7. Dimensionless concentration c' as a function of L' for three-dimensional systems: (a) [Ni–Ni]; (b) [Ni–Ni0.9]; (c) [Ni–Ni0.5]; (d) [Ni–Ni1.5]. The circles and the crosses represent the data points before and after the shape bifurcation, respectively. The solid and dashed lines give the least-square fits of the data points.

fit lines are also plotted in Fig. 6 using solid and dashed lines.

In the elastically homogeneous system [Ni–Ni], shown in Fig. 6(a), the concentration c' at equilibrium varies piecewise-linearly as L' increases and the slope changes as L' passes through the shape bifurcation point L'_c. (Note $L' = L$ in elastically homogeneous cases.) The least-square fit of the (c',L')-pairs gives $c' = 1 + 0.87L'$, for $L' < L'_c \approx 5.6$ or when the equilibrium shape having the minimum total energy is fourfold symmetric. Beyond the supercritical bifurcation point, the concentration obeys a different linear relation, $c' = 1.65 + 0.76L'$, for $L' > 5.6$ where energy-minimizing equilibrium shapes are twofold symmetric. When the mean-

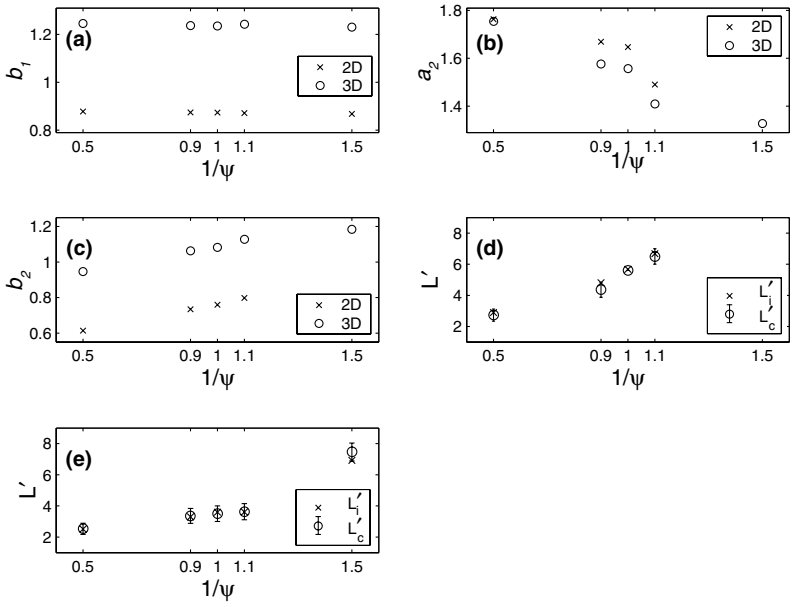

Fig. 8. (a)–(c) The constants in the piecewise linear relation between the normalized concentration c' and L', defined in Eq. (8). (d) The estimation of the shape bifurcation point L'_c (indicated by circles and error bars) and the intersection points of the least-square fitted lines L'_i (labeled by crosses) for two-dimensional systems. (e) Same as (d) except for three-dimensional systems.

field theory of Marqusee [29] is applied with this Gibbs–Thomson equation, the coarsening follows the simple formula, Eq. (2), predicting that coarsening exponent remains 1/3 in the presence of elastic effects and the coarsening rate constant K is proportional to a_2, the c'-axis intercept of (c',L')-lines [28]. Thus, Fig. 6(a) suggests that the coarsening rate constant K increases by a factor of $a_2 = 1.65$ as compared to the stress-free value when the majority of the precipitates attain twofold symmetric shapes, assuming that elastic interactions do not on the average bias coarsening. In this particular case, this result has been verified by 2D large-scale simulations for a system with an area fraction of 10% [26,28]. In the rest of the paper, we make predictions based on this mean-field theory. Whether the elastic interaction term in the Gibbs–Thomson equation can be ignored depends on the system, particularly on the volume fraction and the elastic inhomogeneity.

Next, we consider the concentration c' as the function of L' for a precipitate that is softer than the matrix, [Ni–Ni0.9]. Shown in Fig. 6(b), the computed (c',L')-pairs fall on the two fitted straight lines: $c' = 1 + 0.87L'$, for $L' < L'_c$ and $c' = 1.67 + 0.73L'$, for $L' > L'_c$. The shape bifurcation point L'_c decreases to a value between 3.8 and 4.9 compared with that for the elastically homogeneous system [Ni–Ni], indicating that L'_c decreases when the particle is softer. This is true in both two-dimensional and three-dimensional systems we considered, as shown by the approximate values of the bifurcation point L'_c in Fig. 8(d) and (e), and can be understood intuitively that softer particles are easier to deform and requires less elastic energy to do so. Based on the mean-field theory, the coarsening rate will remain the same for the elastically inhomogeneous system when the average value of L' is less than L'_c if all assumptions in the theory are met. When the precipitates are mostly twofold symmetric, the coarsening rates for the slightly inhomogeneous system [Ni–Ni0.9] and the homogeneous system [Ni–Ni] are comparable, because of the small difference in the c-axis intercepts a_2, 1.67 and 1.65.

In the system [Ni–Ni0.5] where the precipitate is much softer than the matrix, Fig. 6(c) shows that the shape bifurcates at even smaller value of L'_c, lying in the interval (2.3,3.2) and the best fitted lines are given by $c' = 1 + 0.88L'$, for $L' < L'_c$ and $c' = 1.76 + 0.61L'$, for $L' > L'_c$. The larger constant 1.76, compared to 1.65 for the homogeneous system, implies that the coarsening rate based on the piecewise-linear Gibbs–Thomson equation is somewhat faster for systems with elastically softer precipitates when most particles have twofold symmetric shapes. The smaller value of the shape bifurcation point L'_c suggests that the coarsening rate starts increasing at smaller average particle size in the inhomogeneous systems with elastically softer precipitates.

For the case [Ni–Ni1.1], where the precipitate is moderately harder than that of the matrix, the least-square fit yields $c' = 1 + 0.87L'$ for $L' < L'_c$ and $c' = 1.49 + 0.80L'$ for $L' > L'_c$, where L'_c lies in (6.0,7.0). (The figure for this case is omitted.) Beyond the bifurcation point $L' > L'_c$, the c-axis intercept, $a_2 = 1.49$, is clearly smaller than that of the homogeneous case where $a_2 = 1.65$, which is consistent with the previous conclusion: the coarsening rate would be higher for softer precipitates

when most particles attain twofold symmetric shapes. For the case where the precipitate is much harder than the matrix [Ni–Ni1.5], Fig. 6(d) shows that the equilibrium shapes remain fourfold symmetric and c' follows the linear relation $c' = 1 + 0.87L'$ in the range of L' up to 33.1. It's remarkable that, with the definition of L' in Eq. (7), the slope of (c',L')-lines for fourfold symmetric shapes are almost identical and $\approx$0.87. This suggests that there may be a general theory that is valid for homogeneous and inhomogeneous systems with fourfold-symmetric precipitates.

3.4.2. Three-dimensional systems

For three-dimensional systems, Fig. 7 shows that c' again is well approximated by a piecewise-linear function of L' independent of the inhomogeneity in the range of L' examined. Also, the slope of the (c',L')-line changes when the degree of symmetry of the equilibrium shape decreases from cubic (like a cube) to tetragonal (such as a plate or rod, with only one of the coordinate-plane cross-sections being square). The shape bifurcates as L' passes through the bifurcation point L'_c. Despite the vastly different elastic inhomogeneity, from the system with very soft precipitate [Ni–Ni0.5] to that with very hard precipitate [Ni–Ni1.5], the slope of the (c',L')-line for precipitates with the higher symmetry is approximately 1.24 and the differences in the slope among different systems are within the numerical error.

If the mean-field theory of coarsening is extended to three dimensions, the values of the c'-axis intercept of the (c',L')-lines, shown in Fig. 8(b), would imply that the coarsening rate would remain the same as that of systems in the absence of elastic effects if most precipitates in a microstructure have cubic symmetry and elastic-interaction effects are on average small. The coarsening rate would then increase as particle shapes bifurcate, transiting to another power law with the same power, but with a larger constant K when the majority of the precipitates attain tetragonal symmetry. Furthermore, for the systems with softer precipitates, the increase in the coarsening rate would occur at a smaller value of the average L', $\langle L'\rangle$, and the coarsening rate would be higher. Thus, the qualitative behavior for the two- and three-dimensional systems are the same. One notable difference is that, for [Ni–Ni1.5], the bifurcation does not occur up to the largest value of L' of our computations, 33.1, in two dimensions, while the shape of three-dimensional precipitate bifurcates at a moderate value of L', between 6.8 and 8.0.

4. Discussions and conclusions

Qualitatively, the results from the two-dimensional and three-dimensional systems are similar. As the effect of elasticity increases, the equilibrium shape of an isolated precipitate undergoes a bifurcation, from a shape of higher symmetries to that of lower symmetries. In 2D, when elastic effects are sufficiently small, there is a unique equilibrium shape, which is squarish with fourfold symmetries and minimizes the total energy, W_{tot}. When the elastic energy, or equivalently L', is large enough, there are two types of equilibrium shape: one is rectangular with twofold symmetry, is stable and possesses the lowest total energy; the other is fourfold symmetric, stable with respect to fourfold perturbations but unstable to any perturbation with lower symmetry. In 3D, when L' is small, the unique equilibrium shape is cuboidal with cubic symmetry and has the minimum energy; when L' is beyond a critical value, a plate- or rod-like shape with tetragonal symmetry becomes a stable equilibrium shape and posses a smaller total energy. It is difficult to construct a complete bifurcation diagram using the dynamic simulations as described in this work, because the number and location of bifurcation branches are a priori unknown. Other approaches, such as the arc length continuation method, may be more suitable for this purpose and will be pursued in future.

Quantitatively, for the elastically homogeneous system [Ni–Ni], Thompson and Voorhees [16] compared the cross-section in a coordinate plane of a three-dimensional particle at equilibrium with the steady state shape of a two-dimensional particle at the same value of L' and the same area. Recall that L' is identical to L in elastically homogeneous systems. They found good agreement between the (1 0 0)-midpoint cross-section of the three-dimensional particle shape and the corresponding two-dimensional shape at $L' = 2$, but significant differences at $L' = 4$. Also, their results show that the cross-sections of the three-dimensional particles at $L' = 4$ and $L' = 2$ are nearly identical. Here, we compare the equilibrium configurations at values of L' both before and after the bifurcation point using a different scheme: following our method in comparing shapes between different inhomogeneities, we compare the equilibrium shapes for the values of L' resulting in the same ratio of elastic energy, W_e, and surface energy, W_s, for the corresponding reference shape (the unit circle in 2D and the unit sphere in 3D). For [Ni–Ni], the elastic energies of a circular particle and a spherical particle of radius one are 2.77795 and 10.51492, respectively, for $L' = 1$, while the corresponding surface energies are given by 2π and 4π, respectively. Consequently, in Fig. 9, we compare the (1 0 0)-midpoint cross-section of the three-dimensional equilibrium shapes at $L' = 2$ and 5 with the two-dimensional equilibrium shape at $L' = 3.7851$ and 9.4628, respectively, matching the ratio W_e/W_s for the reference configurations. Due to the volume constraint of the three-dimensional precipitate, the cross-sections have the smaller area than π, the area of the two-dimensional particle. For the equilibrium shapes with higher symmetries, shown in Fig. 9(a), the

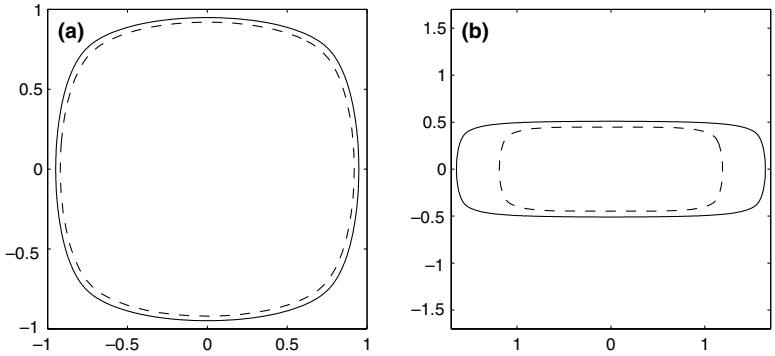

Fig. 9. (a) Comparison of the (100)-midpoint cross-section of the three-dimensional precipitate at equilibrium for $L' = 2$ (the dashed line) and the corresponding two-dimensional particle shape for $L' = 3.7851$ (the solid line). (b) Same as (a) except $L' = 5$ (dashed) and 9.4628 (solid) for the three-dimensional and the two-dimensional particles, respectively.

cross-section of the three-dimensional particle is similar to the contour of the two-dimensional shape. The result is in general agreement with the findings of Thompson and Voorhees [16]. For the equilibrium shapes after the shape bifurcations, Fig. 9(b) shows that the aspect ratio of the cross-section is smaller than that of the two-dimensional particle.

As the precipitate becomes harder, the equilibrium particle shape is more squarish or has a smaller aspect ratio for comparable ratio of elastic and surface energies. Shape bifurcation occurs at larger values of L' for a harder precipitate. In particular, the equilibrium shape for the two-dimensional hard precipitate ([Ni–Ni1.5]) remains fourfold symmetric for L' up to 33.1. In three dimensions, most of the precipitates bifurcate to plate-like shapes when the effect of elasticity increases except that the hard precipitate shape for [Ni–Ni1.5] becomes rod-like instead of plate-like for large values of L'. The appearance of a rod at higher L' after a plate-like shape at a lower L' for a very hard particle is intriguing. It indicates that the elastic-energy minimizing shape of a domain harder than the matrix is an infinitely long rod, rather than an infinitely thin plate predicted for elastically homogeneous systems. Our result is consistent with the bifurcation theory of Johnson et al. [36] predicting that, restricting precipitates to be spheroids, a prolate spheroid could be global energy minimizer for cubic materials when the particle size is large enough.

With regard to the interface concentration at equilibrium, we find that, independent of the dimensionality (2D or 3D) and elastic inhomogeneity of the system, the concentration at equilibrium is well approximated by a piecewise linear function of L' for the range of L' examined and that the slope of this function decreases at the shape bifurcation point. Furthermore, before the shape bifurcation, the slope of the linear relation changes little under the new parameter L', given in Eq. (7), as the elastic inhomogeneity varies from soft precipitate to hard precipitate. Because the slope changes near the bifurcation point, the critical value of shape bifurcation L'_c can be estimated by the intersection of the two linear functions before and after the bifurcation, L'_i in Eq. (9).

Given the Gibbs–Thomson equation, the mean-field theory of Thornton et al. [26], based on Marqusee's for stress-free systems [29], can now be extended to elastically inhomogeneous and/or three-dimensional cases. The predictions are made for two limits where $\langle L \rangle$ is well below the bifurcation point and most particles remain fourfold or cubic symmetric and where $\langle L \rangle$ is well over the bifurcation point and most particles have undergone shape bifurcation. Our numerical results combined with the theory predict the coarsening exponent remains 1/3 for both cases, while the rate constant is expected to be the stress-free value at the limit where most particles are fourfold or cubic symmetric, but increases to a calculated value when particles are mostly twofold or tetragonal symmetric. The change in the rate constant is most significant when particle are softer than the matrix. It is remarkable that our results suggest that elastic stress have no effect on coarsening kinetics in systems where most particles have not undergone shape bifurcation, regardless of the dimensionality and the elastic inhomogeneity.

In this theory, the interparticle elastic interactions, which depend on the volume fraction of the particle phase and the elastic inhomogeneity, are assumed negligible in biasing coarsening kinetics. As discussed earlier, this assumption is valid when the volume fraction is sufficiently small. Let c'_{Ie} denote the portion of the concentration that is included in the Gibbs–Thomson equation (1), which accounts for the effects of both interparticle elastic interactions and the shape distortion from the equilibrium shape in isolation. Taken from Thornton et al. [28], Fig. 10 shows c'_{Ie} for a 2D, elastically homogeneous system with the average value of L, $\langle L \rangle$, at 7.1 and area fraction of the particles at 10%. Each solid point in the figure records the value of c'_{Ie} averaged over an individual particle, plotted against L of the particle.

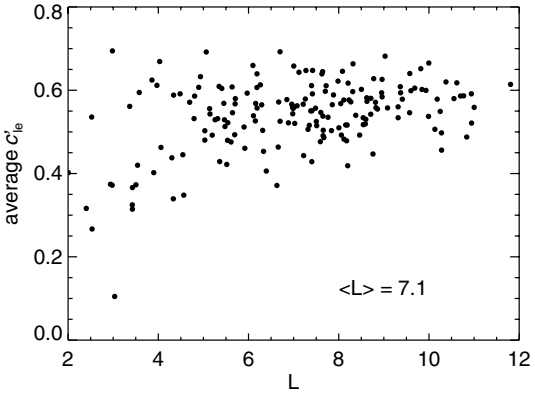

Fig. 10. The portion of concentration that is not accounted for by the Gibbs–Thomson equation (1) of isolated particles averaged over the interface of each particle plotted against the individual particle's L. The result is obtained from a simulation of an elastically homogeneous, many-particle system. The figure is reproduced from [28].

From Fig. 10, the average c'_{Ie} scatters around a constant for a wide range of L (or particle size), or at most is a weak function of the particle size. The result suggests that interparticle elastic interactions do not affect the overall coarsening kinetics in this case. There is a large body of evidence that indicates elastic interactions could have significant effects on coarsening at higher volume fractions, as the interactions become stronger with decreasing distances between particles. The average behavior of c'_{Ie} as a function of particle size provides the extra term required in a theory for coarsening in elastically stressed systems where interparticle elastic interactions modify the coarsening kinetics. Development of such a term is beyond the scope of this paper but is planned in the near future.

One of our objectives is to compare the prediction of theory with the experimental results. However, to date, there has been little experimental work examining the kinetics of coarsening based on the equivalent radii of the particles for the range of L' large enough to cause shape bifurcation. The difficulty is caused by the measurement of the equivalent radius, which requires volumetric information of the individual particles and thus three-dimensional reconstructions of a sufficiently large number of particles. Since experiments involving three-dimensional reconstructions are time and labor intensive, the currently available experimental data are instead obtained by imaging two-dimensional cross-sections. When particles are non-equiaxed, the cross-sectional area of particle does not necessarily reflect the true volume of the particle. Thus, many experiments focus on characterizing the kinetics when particles are approximately equiaxed (see, for example, [37–40]). To account for non-equiaxed particle shapes, one could use another length scale that characterizes the evolution of a coarsening system: the inverse of the surface area per unit volume measured on off-$\langle 1\,0\,0\rangle$-direction cuts.

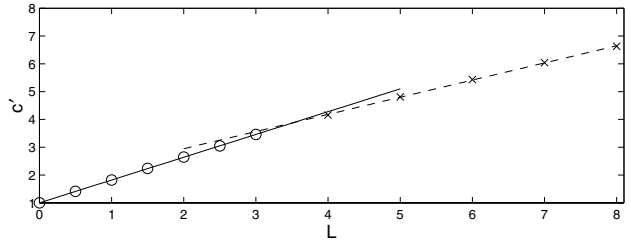

Fig. 11. The concentration c' at stable equilibrium as L varies for the two-dimensional [Ni–Ni_3Ga] system.

Since this length scale is different from the equivalent particle radius used in the theory and computer simulations, a direct comparison cannot be made between the experimental results and the theoretical predictions made in this paper. For bifurcated particles, only qualitative comparisons have been made between experimental results and a 2D large-scale simulation [41]. For a quantitative comparison, we require the volumetric information for sufficiently large number of particles in samples that are annealed for various time intervals. Also, the volume fraction in such experiments must be chosen so that elastic interactions do not alter the coarsening kinetics, as mentioned earlier.

In this paper, a new dimensionless parameter L', defined in Eq. (4), is introduced to represent the characteristic ratio between elastic and surface energy of an elastically inhomogeneous system. To demonstrate the difference between L' and L defined earlier in [7], we compare the ratio of elastic to surface energies for a spherical precipitate of unit radius in an infinite matrix, denoted by R_e. For $L = 1$, in the special cases where C^P is proportional to C^M, the value of the ratio R_e varies from 0.60390 for the system [Ni–Ni0.5] to 0.96019 for [Ni–Ni1.5]; in more realistic cases, R_e increases from 0.76894 for the inhomogeneous system [Ni–Ni_3Ga] where a soft precipitate (Ni_3Ga) is embedded in the matrix Ni phase, to 0.94992 for [Ni–Ni_3Si] with a hard precipitate (Ni_3Si). [2] In contrast, for the same value of L' defined as in Section 2, the ratio R_e remains constant independent of the elastic inhomogeneity of the system.

Finally, we demonstrate that the validity of the piecewise linear approximation is not due to the special correlation between the elastic constants of the precipitate and the matrix studied in this paper where C^P is proportional to C^M. Fig. 11 shows the normalized concentration at stable equilibrium as a function of L for the two-dimensional inhomogeneous system [Ni–Ni_3Ga], where a soft precipitate (Ni_3Ga) is embedded in the matrix Ni phase. Clearly, the piecewise linear approximation between c and L remains valid in the realistic systems.

[2] The three independent elastic constants, normalized by c_{44} of Ni, are given by $c_{11} = 1.54$, $c_{12} = 0.996$ and $c_{44} = 0.87$ for Ni_3Ga, and $c_{11} = 3.04$, $c_{12} = 1.62$ and $c_{44} = 1.35$ for Ni_3Si [42].

Acknowledgements

The authors thank Dr. V. Cristini for providing the adaptive surface mesh package for this research and Dr. P. Leo for helpful discussions. The numerical simulations were done on two Beowulf clusters acquired with NSF-SCREMS funding at Illinois Institute of Technology and University of California at Irvine. K.T. and P.W.V. are grateful for the financial support of the NSF under Grant #9707073. J.L. acknowledges the support of the NSF Division of Mathematical Sciences.

References

[1] Taylor JE. Crystalline variational problems. Bull Am Math Soc 1978;84:568–88.
[2] Fonseca I. The Wulff theorem revisited. Proc R Soc Lond A 1991;432:125–45.
[3] Johnson CA, Chakerian GD. On proof uniqueness of Wulffs construction of shape of minimum surface free energy. J Math Phys 1965;6:1403–4.
[4] Lee JK, Aaronson HI, Russell KC. On the equilibrium shape of a non-centro-symmetric gamma plot. Surf Sci 1975;51:302–4.
[5] Arbel E, Cahn JW. On invariances in surface thermodynamic properties and their applications to low symmetry crystals. Surf Sci 1975;51:305–9.
[6] Thompson ME, Su CS, Voorhees PW. The equilibrium shape of a misfitting precipitate. Acta Metall Mater 1994;42:2107–22.
[7] Voorhees PW, McFadden GB, Johnson WC. On the morphological development of second-phase particles in elastically stressed solids. Acta Metall Mater 1992;40:2979–92.
[8] Jou HJ, Leo PH, Lowengrub JS. Microstructural evolution in inhomogeneous elastic media. J Comput Phys 1997;131:109–48.
[9] Schmidt I, Gross D. The equilibrium shape of an elastically inhomogeneous inclusion. J Mech Phys Solids 1997;45: 1521–49.
[10] Schmidt I, Mueller R, Gross D. The effect of elastic inhomogeneity on equilibrium and stability of a two particle morphology. Mech Mater 1998;30:181–96.
[11] Leo P, Lowengrub J, Nie Q. Microstructural evolution in orthotropic elastic media. J Comput Phys 2000;157:44–88.
[12] Onaka S. Averaged Eshelby tensor and elastic strain energy of a superspherical inclusion with uniform eigenstrains. Phil Mag Lett 2001;81:265–72.
[13] Onaka S, Kobayashi N, Fujii T, Kato M. Simplified energy analysis on the equilibrium shape of coherent gamma' precipitates in gamma matrix with a superspherical shape approximation. Intermetallics 2002;10:343–6.
[14] Onaka S, Kobayashi N, Fujii T, Kato M. Energy analysis with a superspherical shape approximation on the spherical to cubical shape transitions of coherent precipitates in cubic materials. Mat Sci Eng A Struct 2003;347:42–9.
[15] Johnson WC, Cahn JW. Elastically induced shape bifurcations of inclusions. Acta Metall 1984;32:1925–33.
[16] Thompson ME, Voorhees PW. Equilibrium particle morphologies in elastically stressed coherent solids. Acta Metall Mater 1999;47:983–96.
[17] Mueller R, Gross D. 3D simulation of equilibrium morphologies of precipitates. Comp Mater Sci 1998;11:35–44.
[18] Mueller R, Gross D. 3D inhomogeneous, misfitting second phase particles-equilibrium shapes and morphological development. Comp Mater Sci 1999;16:53–60.
[19] Mueller R, Gross D. 3D equilibrium shapes of misfitting precipitates in anisotropic materials. Z Angew Math Mech 2000;80(Suppl 2):S397–8.
[20] Eckert S, Mueller R, Gross D. 3D equilibrium shapes of periodically arranged anisotropic precipitates with elastic misfit. Arch Mech 2000;52:663–83.
[21] Eckert S, Gross D, Mueller R. 3D periodic arrangement of misfitting precipitates in anisotropic materials. Z Angew Math Mech 2001;81(Suppl 2):S283–4.
[22] Zhu JZ, Liu ZK, Vaithyanathan V, et al. Linking phase-field model to CALPHAD: application to precipitate shape evolution in Ni-base alloys. Scripta Mater 2002;46:401–6.
[23] Li XF, Lowengrub J, Nie Q, Cristini V, Leo P. Microstructure evolution in three-dimensional inhomogeneous elastic media. Metall Mater Trans 2003;34A:1421–31.
[24] Cristini V, Blawzdzieweicz J, Loewenberg M. An adaptive mesh algorithm for evolving surfaces: simulations of drop breakup and coalescence. J Comp Phys 2001;168:445.
[25] Christian JW. The theory of transformations in metals and alloys, part I and II Oxford, England: Pergamon Elsevier Science; 2002.
[26] Thornton K, Akaiwa N, Voorhees P. Dynamics of late-stage phase separation in crystalline solids. Phys Rev Lett 2001;86:1259–62.
[27] Thornton K, Akaiwa N, Voorhees P. Large-scale simulations of ostwald ripening in elastically stressed solids: I. development of microstructure. Acta Mater 2004;52:1353–64.
[28] Thornton K, Akaiwa N, Voorhees P. Large-scale simulations of ostwald ripening in elastically stressed solids: II. coarsening kinetics and particle size distribution. Acta Mater 2004;52:1365–78.
[29] Marqusee JA. Dynamics of late stage phase separations in 2 dimensions. J Chem Phys 1984;81:976–81.
[30] Marqusee JA, Ross J. Theroy of ostwald ripening: competitive growth and its dependence on volume fraction. J Chem Phys 1984;80:536–43.
[31] Voorhees PW, McFadden GB, Boisvert RF, Meiron DI. Numerical-simulation of morphological development during ostwald ripening. Acta Metall 1988;36:207–22.
[32] Voorhees PW. Ostwald ripening of 2-phase mixtures. Annu Rev Mater Sci 1992;22:197–215.
[33] Leo PH. The effect of elastic fields on the morphological stability of a precipitate grown from solid solution. PhD thesis, Carnegie Mellon University; 1987.
[34] Roitburd AL. Equilibrium of crystals formed in the solid state. Sov Phys Dokaldy 1971;16:305–8.
[35] Khachaturyan AG. Some questions concerning the theory of phase transformations in solids. Sov Phys Solid State 1967;8:2163–8.
[36] Johnson WC, Berkenpas MB, Laughlin DE. Precipitate shape transitions during coarsening under uniaxial stress. Acta Metall 1988;36:3149–62.
[37] Cho JH, Ardell AJ. Coarsening of Ni_3Si precipitates in binary Ni–Si alloys at intermediate to large volume fractions. Acta Mater 1997;45:1393–400.
[38] Cho JH, Ardell AJ. Coarsening of Ni_3Si precipitates at volume fractions from 0.03 to 0.30. Acta Mater 1998;46:5907–16.
[39] Kim DM, Ardell AJ. The volume-fraction dependence of Ni_3Ti coarsening kinetics – new evidence of anomalous behavior. Scripta Mater 2000;43:381–4.
[40] Kim DM, Ardell AJ. Coarsening of Ni_3Ge in binary Ni–Ge alloys: microstructures and volume fraction dependence of kinetics. Acta Mater 2003;51:4073–82.
[41] Lund AC, Voorhees PW. The effects of elastic stress on coarsening in the Ni–Al system. Acta Mater 2002;50:2085–98.
[42] Prikhodko SV, Carnes JD, Isaak DG, Ardell AJ. Elastic constants of a Ni-12.69 at.% Al alloy from 295 to 1300 k. Scripta Mater 1997;38:67–72.